

PAPER

## Neoclassical transport due to resonant magnetic perturbations in DIII-D

To cite this article: Priyanjana Sinha *et al* 2022 *Nucl. Fusion* **62** 126028

View the [article online](#) for updates and enhancements.

### You may also like

- [Impact of resonant magnetic perturbations on the L-H transition on MAST](#)  
R Scannell, A Kirk, M Carr et al.
- [Effect of resonant magnetic perturbations on local plasma current density gradients and neoclassical tearing modes](#)  
Q. Yu, S. Günter and K. Lackner
- [Research on the effect of resonant magnetic perturbations on disruption limit in J-TEXT tokamak](#)  
Qiming Hu, Nengchao Wang, Q Yu et al.

# Neoclassical transport due to resonant magnetic perturbations in DIII-D

Priyanjana Sinha<sup>1,\*</sup>, Nathaniel M. Ferraro<sup>1</sup> and Emily Belli<sup>2</sup>

<sup>1</sup> Princeton Plasma Physics Laboratory, Princeton, NJ 08543-0451, United States of America

<sup>2</sup> General Atomics, San Diego, CA 92186-5608, United States of America

E-mail: [psinha@pppl.gov](mailto:psinha@pppl.gov)

Received 14 May 2021, revised 13 September 2022

Accepted for publication 23 September 2022

Published 17 October 2022



CrossMark

## Abstract

The role of neoclassical physics in the particle and energy transport during the application of resonant magnetic perturbations (RMPs) to suppress the edge localised modes in a tokamak is analysed. The neoclassical fluxes in non-axisymmetric DIII-D equilibria with applied RMPs are calculated using the NEO code. The magnetic field provided to NEO as an input is calculated using M3D-C1 and includes the nonlinear one-fluid plasma response. Neoclassical fluxes obtained in this study are found to dramatically increase in the presence of applied RMPs, and are in same range as the total radial particle fluxes calculated in comparable RMP discharges in DIII-D [1]. This suggests that neoclassical transport plays a significant role in edge transport when RMPs are present. An increase in neoclassical fluxes during the edge-localized mode suppressed phase in DIII-D plasmas is calculated and is strongly correlated with the observation of density pump-out in the experiment.

Keywords: neoclassical transport, M3D-C1, NEO, DIII-D, density pump-out, RMP, MHD

(Some figures may appear in colour only in the online journal)

## 1. Introduction

The high confinement regime (H-mode) [2, 3] in a tokamak is characterized by a steep pressure gradient at the edge. These gradients often cause instabilities in the plasma known as edge-localized modes (ELMs), which result in periodic bursts of particles and energy onto the plasma facing components (PFC) [4–6]. This could cause an accelerated degradation of PFC and hence, should be avoided. One of the methods to eliminate or control the ELMs is by applying RMPs [7–9]. This technique perturbs the local magnetic field in the pedestal region and generates a plasma response that is frequently marked by a reduction in the pedestal density, also known as density pump-out [10–12]. In some cases, this process can also significantly reduce central plasma density [13] which is detrimental to fusion performance. It is therefore crucial to understand the transport mechanisms that governs density pump-out for better plasma performance in RMP-ELM suppression experiments.

Much progress has been made on understanding the plasma response to resonant magnetic perturbations (RMPs) and on

the conditions for peeling-ballooning stability. However, the transport properties of perturbed tokamak equilibria and the associated relaxation of kinetic profiles (density, temperature, and rotation) remains poorly understood. Without such an understanding, extrapolating the effects of RMPs on plasma performance and on ELM suppression to reactor-scale tokamaks cannot be done with confidence, especially due to the complexity of the observed phenomenology. Recent progress in this area has been encouraging; indeed, there are a variety of calculations that have been carried out with distinctly different physics models, each finding enhanced particle transport in the presence of 3D fields. Density pump-out has been observed in nonlinear calculations using the TM1 code [12], which implements a reduced two-fluid model in simplified geometry, due to increased radial transport caused by the formation of magnetic islands. This effect may be related to flutter transport [14], which has also been examined using analytic models applied to field perturbations calculated by M3D-C1. Quasi-linear modelling with MARS-Q [15] using a linear, resistive plasma response model has found that the nonambipolar transport associated with neoclassical toroidal viscosity (NTV) can

\* Author to whom any correspondence should be addressed.

also lead to density pump-out. At higher fidelity, calculations of neoclassical and turbulent transport have been carried out with XGC [16] using perturbed fields calculated by M3D-C1. These calculations also find transport levels comparable to empirical observations of pump-out; however, these calculations are computationally expensive and have not yet been carried to ion transport timescales. Experimentally [17–19], it has been observed that density fluctuations increase in the presence of RMPs, a possible enhancement of turbulent transport. However, turbulence modelling does not show clear support for the hypothesis that pump-out can be explained by changes to microstability due to RMPs [20].

In this paper, we demonstrate an efficient method for calculating the steady-state neoclassical fluxes using a realistic, nonlinear plasma response model. The nonaxisymmetric magnetic geometry is found using the extended magnetohydrodynamic (MHD) code M3D-C1 [21, 22] by calculating the plasma response to applied 3D fields, using physically realistic diverted geometry, dissipation, and sources. The neoclassical transport is then calculated in this 3D geometry using NEO [23]. We show here that the calculated neoclassical fluxes are enhanced significantly by the presence of nonaxisymmetric fields and correlate strongly with the observations of pump-out in DIII-D experiments. We also find that even at modest RMP levels, the linear plasma response can differ sufficiently from that of nonlinear response calculations and that the calculated neoclassical fluxes can differ significantly.

## 2. Numerical tools

### 2.1. NEO

RMPs give rise to a non-axisymmetric equilibrium. The non-axisymmetric perturbations will result in changes to the neoclassical transport, and will break the intrinsic ambipolarity of transport in axisymmetry. The NEO code with an improved capability to handle non-axisymmetric geometry has been used in this work to calculate the neoclassical transport arising in non-axisymmetric equilibria [24].

NEO calculates the neoclassical fluxes solving the standard drift kinetic equation (DKE) supplemented with a Poisson equation [23, 24]. The DKE is expanded in powers of  $\rho_*i$  defined as the ratio of the ion gyroradius to system size. The code does not account for higher-order drift terms or the tangential magnetic drift. NEO uses the full linearized Fokker–Planck multi-species collisional operator to calculate the inter-species coupling and the neoclassical transport over a range collisionality [25]. The second order neoclassical particle and energy fluxes are computed in NEO using:

$$\Gamma_a = \left\langle \int d^3v g_{1a} v_D \cdot \nabla r \right\rangle \quad (1)$$

$$Q_a = \left\langle \int d^3v m_a \epsilon g_{1a} v_D \cdot \nabla r \right\rangle, \quad (2)$$

where  $a$  is the species index,  $g_{1a}$  is the non-adiabatic distribution,  $\epsilon = v_{\parallel}^2/2 + \mu B = v^2/2$  is the kinetic energy per unit mass,  $\mu = v_{\perp}^2/2B$  is the magnetic moment,  $v_D \cdot \nabla r =$

$\frac{v_{\parallel} + \mu B}{\Omega_{ca} B} \mathbf{b} \times \nabla B \cdot \nabla r$ , where  $\Omega_{ca}$  is the cyclotron frequency, and  $\langle a \rangle$  is the standard flux-surface average of  $a$ . For more details see references [23, 24].

The surface geometry and pressure gradient at various radii is provided by M3D-C1 (this is discussed in more detail in the following section), and then local nonaxisymmetric MHD equilibria are constructed using the Le3 code [26]. The routine maps the contours of  $R(\psi, \theta, \phi)$  and  $Z(\psi, \theta, \phi)$  from M3D-C1 as a sum of Fourier coefficients,

$$R(r, \bar{\theta}, \phi) = \sum_{m=0}^{N_{\theta}} \sum_{n=0}^{N_{\phi}} \sin(m\theta) [a_{mn}^r \cos(n\phi) + b_{mn}^r \sin(n\phi)] \\ + \cos(m\theta) [c_{mn}^r \cos(n\phi) + d_{mn}^r \sin(n\phi)] \quad (3)$$

$$Z(r, \bar{\theta}, \phi) = \sum_{m=0}^{N_{\theta}} \sum_{n=0}^{N_{\phi}} \sin(m\theta) [a_{mn}^z \cos(n\phi) + b_{mn}^z \sin(n\phi)] \\ + \cos(m\theta) [c_{mn}^z \cos(n\phi) + d_{mn}^z \sin(n\phi)]. \quad (4)$$

Here  $\bar{\theta}(r, \theta, \phi)$  is a parametric angle which can be related to the straight field line angles (in axisymmetric geometry, it is equivalent to the Miller poloidal arc length). In this case, good convergence with the M3D-C1 equilibria was obtained with  $N_{\theta} = 15$  in the core and between  $25 < N_{\theta} < 30$  in the edge, and  $N_{\phi} = 3$  in DIII-D discharge #160921 and  $N_{\phi} = 2$  in DIII-D discharge #158115. Le3 then takes as input the numerical ( $R, Z$ ) Fourier coefficients and their radial derivatives for a specified surface and constructs the local, ideal equilibria, subject to the constraints of zero radial current and radial force balance. These local equilibria are then used by NEO to calculate the neoclassical transport. The numerical resolution for the NEO simulations performed here uses  $N_{\xi} = 16$ , number of polynomials to describe the distribution function and the resolution in the  $\theta$  direction ( $N_{\theta}$ ) is same as that used in Le3 code.

When the magnetic field is non-axisymmetric, the intrinsic ambipolarity of the neoclassical fluxes is lost, typically with ion fluxes exceeding electron fluxes. Nonambipolar fluxes cannot persist in steady-state, as they necessarily imply a time-dependent electric field. In strongly non-axisymmetric systems such as stellarators, these nonaxisymmetric fluxes cannot be compensated by other physical mechanisms such as turbulence, and therefore ambipolarity can only be restored through the evolution of  $E_r$  to the neoclassical offset value (i.e. the value at which the neoclassical fluxes are ambipolar). However, Calvo *et al* in reference [27] showed that when nonaxisymmetric perturbations are sufficiently small, nonambipolar fluxes from turbulence are competitive with the neoclassical fluxes, and  $E_r$  is not constrained to be the neoclassical offset value. The criterion for being in this regime of small perturbations is that  $\delta B/B_0 < \sqrt{\rho_i/L}$  where  $L$  is the equilibrium gradient length scale. Tokamak RMPs fall comfortably in this regime, and it is indeed observed that  $E_r$  is generally very different from the neoclassical offset value. A full accounting of the evolution of the radial electric field and the restoration of ambipolarity would therefore require turbulence calculations

carried out at least to second order in the gyrokinetic ordering [28]. However, the estimate of nonambipolar turbulent flux in Calvo *et al* is significantly smaller than the nonambipolar neoclassical fluxes that we calculate. Perhaps more importantly, the input momentum from neutral beam injection is large (on the order of a few N m), and this momentum source can itself balance nonambipolar neoclassical flux [29]. This suggests that the radial electric field here is best calculated as a balance between the input momentum density and the NTV. To resolve these issues are very challenging and well beyond the scope of this paper. In the absence of such a calculation, the only justifiable choice for  $E_r$  in our analysis is that which is determined empirically, which is what we use in our calculations. The resulting nonambipolar neoclassical fluxes are not facially unphysical, but rather just an incomplete piece of the total transport which must be ambipolar only in aggregate.

## 2.2. M3D-C1

M3D-C1 [21] is a finite-element fluid code for solving extended-MHD models. It uses a non-uniform, unstructured grid that ensures the continuity of scalar fields and their first-derivatives across element boundaries [30]. The computational domain for the code extends beyond the last closed flux surface and includes the open field line region [22].

For this work, we have considered the single-fluid extended-MHD model (for more details see references [21, 31, 32]) i.e. we assume all charged species (electrons and ions) to have the same fluid velocity  $v$ . This assumption is made here for convenience due to the numerical challenges introduced by two-fluid effects. We leave the exploration of the two-fluid effects as future work.

For the single fluid MHD calculations performed here, density, momentum, and energy are introduced into the system using an idealized axisymmetric neutral beam source. The particle, momentum, and heat sources are Gaussians with centre (1.7, 0) and variance 0.2, and the total rates of particle, torque, and heat injection are  $1.0 \times 10^{22}$  ions  $s^{-1}$ , 430 N m, and 1.1 GW respectively.

The diffusion coefficient ( $D$ ) and, the heat flux coefficient ( $\kappa$ ) profiles are chosen to balance these sources for the initial axisymmetric density, momentum, and temperature profile. In these single fluid M3D-C1 calculations, the adiabatic index ( $\Gamma$ ) is taken as 1.67, a Spitzer resistivity model is used, and the coefficient of viscosity ( $\mu$ ) is taken as  $3.65 \times 10^{-4}$  N s  $m^{-2}$ . The values of the above mentioned coefficients used in M3D-C1 for the present study are close to their inferred anomalous values in the experiment.

The calculated plasma response self-consistently includes the non-axisymmetric changes in response to the magnetic field, current density, density, pressure and rotation to the externally applied perturbed field. When considering the impact of the non-axisymmetric field on transport, it is imperative to include this self-consistent non-axisymmetric plasma response because the currents associated with the response can dramatically alter the spectrum of the magnetic field.

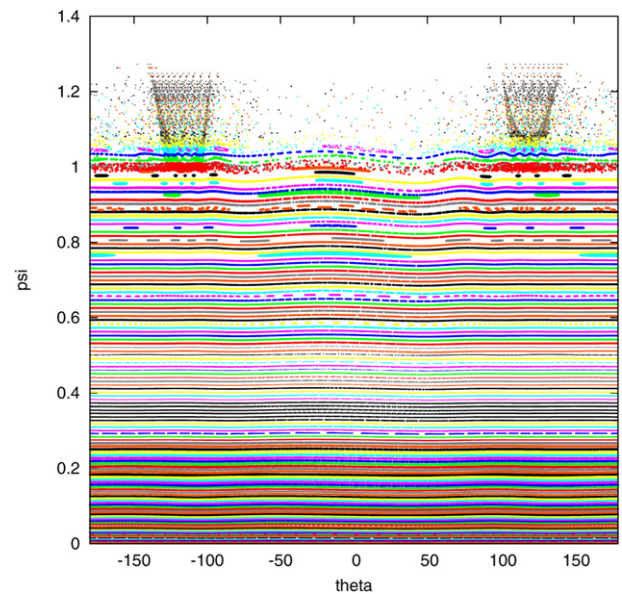


**Figure 1.** Poincaré plot for the linear M3D-C1 run for DIII-D shot #160921 for  $I_{RMP} = 6$  kA at  $t = 5110$  ms.

## 2.3. Workflow

The RMP field applied perturbs the magnetic flux surfaces and displaces them from their initial location. Because resistivity is included in this response model, the perturbed field also includes magnetic islands and regions of stochasticity, although these regions are typically small because the plasma response generally strongly opposes island formation. Figure 1 shows the magnetic surfaces for DIII-D shot #160921 at 5110 ms and  $I_{RMP} = 6$  kA. It is visible that towards the edge of the plasma the magnetic field becomes stochastic. As previously mentioned, NEO requires the existence of closed surfaces to calculate neoclassical transport. We therefore use the  $T_e$  isotherms in M3D-C1 to represent the surface geometry. In regions of magnetic islands or stochasticity, these isotherms capture the kink-like (nonresonant) distortions of the surface, but do not capture the tearing-like (resonant) perturbations. These isotherms are guaranteed to be closed surfaces and are essentially identical to the magnetic surfaces where magnetic surfaces exist. Figure 2 shows the isotherms calculated for DIII-D shot #160921 with  $I_{RMP} = 6$  kA in the I-coils, with the normal displacements of the isotherms scaled by an additional factor of four for visibility.

This technique of course limits the physical accuracy of the neoclassical calculation in magnetic islands or stochastic regions, but it is at this time the best we are able to do without resorting to global drift-kinetic formulations, which are significantly more computationally expensive and not generally available in practice. A discussion about possible physics that we are excluding in our flux calculations by making such an approximation is presented in section 4. It should be noted that the geometry of the perturbed isotherms is a nonlinear function of the perturbed temperature, and therefore will scale nonlinearly with the RMP amplitude. In section 3.1 it is shown



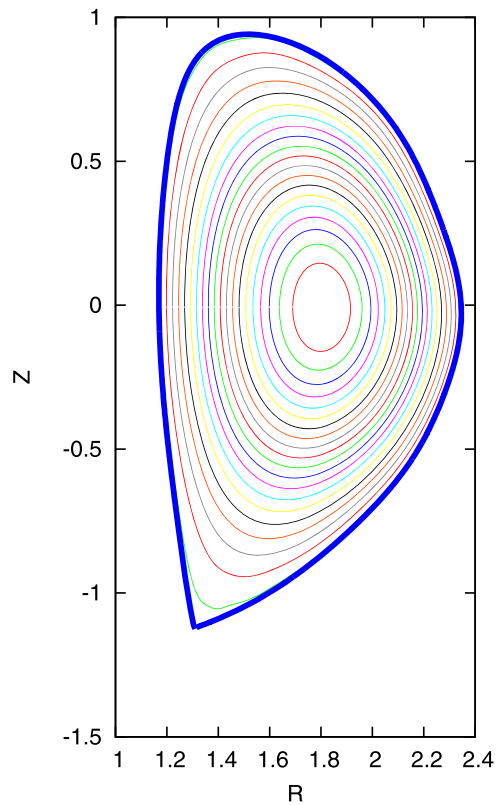


**Figure 2.** Isotherm surfaces at different  $\psi_{\text{norm}}$  values for the linear M3D-C1 run for DIII-D shot #160921 for  $I_{\text{RMP}} = 6$  kA at  $t = 5110$  ms. The thicker blue curve represents  $\psi = 1$  surface.

that this nonlinear behaviour is observed at (or above) modest values of RMP amplitude. Since a linear plasma response model does not capture this nonlinear physics, it is likely give us incorrect results.

The isotherms are used as input into Le3, which then constructs a series of local force-balance equilibria that can be used as input to NEO code. NEO then calculates the neoclassical transport fluxes.

### 3. Neoclassical fluxes in DIII-D discharges with RMP

DIII-D [33] uses a set of 12 in-vessel perturbation coils called I-coils (six upper and six lower) to control ELMs. The dominant toroidal mode number in RMP ELM suppression experiments on DIII-D is typically  $n = 2$  or  $n = 3$ . For  $n = 2$ , the phase between I-coils rows can be varied continuously which gives rise to a broad range of poloidal spectra [11, 34]. The two DIII-D discharges analysed in this work #160921 and #158115 are discussed in detail in reference [35] and references [11, 36], respectively. These two discharges are informative because they are well-diagnosed cases covering both  $n = 2$  response for a range of poloidal RMP spectrum (#158115) and  $n = 3$  response including sustained periods of ELM suppression in DIII-D's ITER Baseline Scenario (IBS) (#160921). The simulations performed in this work assume a pure plasma with an equal electron and ion density.

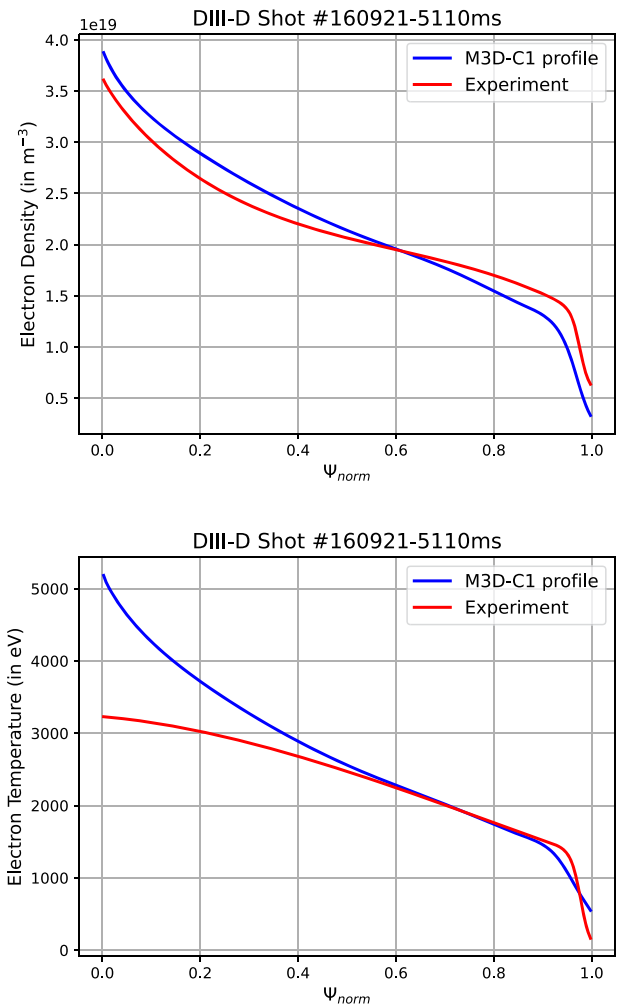


**Figure 3.** Comparison of electron density profile (top) and electron temperature profile (bottom) used in linear and nonlinear M3D-C1 runs (in blue) with the experimental profiles (in red) for DIII-D shot #160921 at  $t = 5100$  ms.

#### 3.1. DIII-D discharge #160921

The motivation behind the experiment was to assess the level of ELM control that could be achieved in the IBS. Only the upper I-coil current was operated with  $n = 3$  and  $I_{\text{RMP}} = 6$  kA. The input torque was stepped up from 3.5 N m to 5 N m between  $t = 4400$  ms and  $t = 4700$  ms, leading to suppression of ELMs [35]. For our analysis, we have selected a RMP ELM-suppressed time slot 5100 ms with the toroidal magnetic field  $B_T = 1.6$  T, line averaged density  $\langle n_e \rangle = 2.4 \times 10^{19} \text{ m}^{-3}$ , plasma current  $I_p = 1.2$  MA,  $q_{95} = 3.2$ , and  $\beta_N = 1.9$ . Model density and temperature profiles consistent with the density and heat sources (see figure 3) were used for the linear and nonlinear M3D-C1 runs performed to obtain the perturbed equilibrium for the time slot 5100 ms, which is then analysed using NEO to study the neoclassical properties. Both linear and nonlinear calculations were done in order to better understand how the linear response deviated from the nonlinear response as the RMP amplitude was increased. These model profiles differ from the empirical fits because we have imposed the constraints  $n_e = n_i$  and  $T_e = T_i$  in our model (which is not true

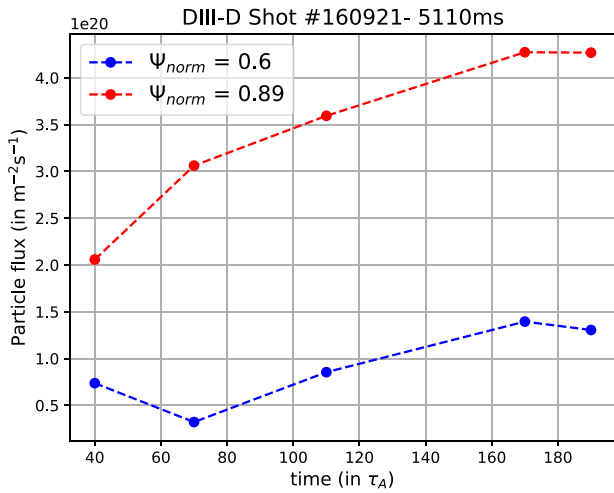


**Figure 4.** Neoclassical particle flux of ions at different time slices (where  $\tau_A$  is Alfvén time) at  $\psi_{norm} = 0.6$  (in blue) and  $\psi_{norm} = 0.89$  (in red) calculated by NEO for DIII-D shot #160921 using nonlinear M3D-C1 equilibrium at time slot 5100 ms for  $I_{RMP} = 6$  kA.

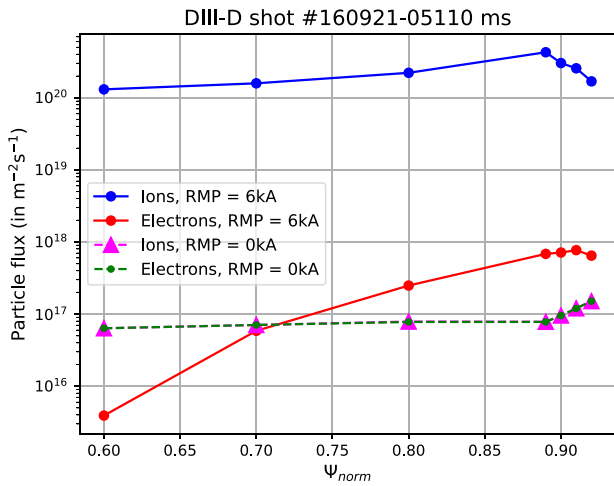


**Figure 5.** Neoclassical particle flux of electrons (in red) and ions (in blue) calculated by NEO for DIII-D shot #160921 using the equilibrium calculated by nonlinear M3D-C1 at time slot 5100 ms for  $I_{RMP} = 6$  kA. The axisymmetric particle flux limit ( $I_{RMP} = 0$  kA) for ions (in magenta triangle markers) and electrons (in green dashed line) calculated by NEO for the same shot at 5100 ms.

in the empirical fits), and because fast beam ions constitute a significant fraction of the core pressure in the experiment. In the model, there is no separate beam ion species, so this additional pressure is represented as a higher core temperature so that the total pressure in the model remains identical to the total pressure in the empirical reconstruction. The choice to match pressure rather than matching temperature was made because the plasma response depends directly on pressure but only indirectly on temperature (through resistivity) in this single-fluid model.

To ensure that the nonlinear MHD calculations for DIII-D shot #160921 at  $I_{RMP} = 6$  kA reached a steady state, the neoclassical fluxes were calculated at different times in the simulation as shown in figure 4. It can be seen that towards

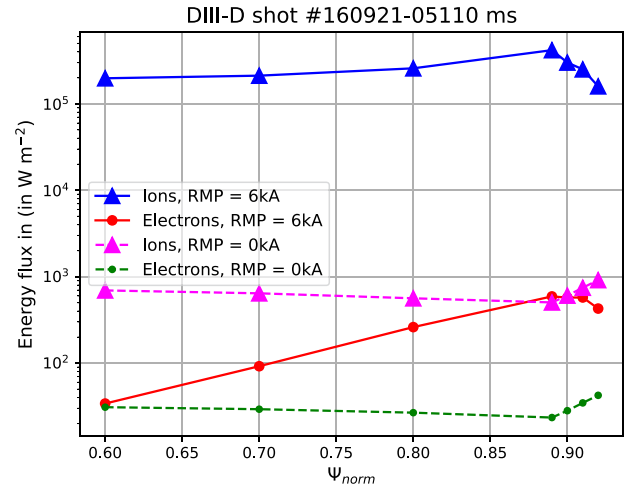


**Figure 6.** Neoclassical energy flux of electrons (in red) and ions (in blue) calculated by NEO for DIII-D shot #160921 using the equilibrium calculated by nonlinear M3D-C1 at time slot 5100 ms for  $I_{RMP} = 6$  kA. The axisymmetric particle flux limit ( $I_{RMP} = 0$  kA) for ions (in magenta) and electrons (in green) calculated by NEO for the same shot at 5100 ms.

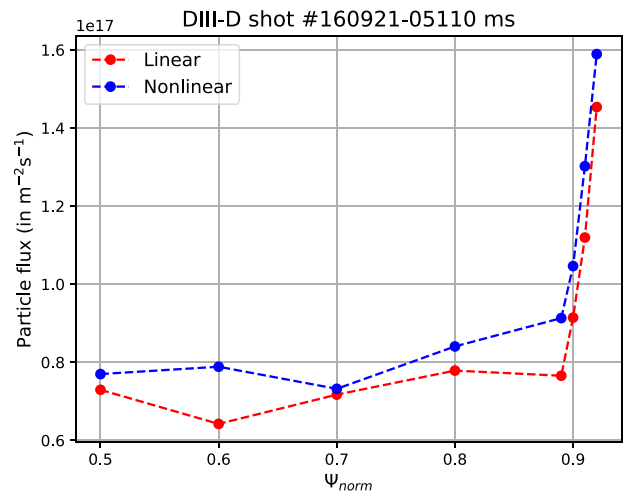


**Figure 7.** Neoclassical particle flux for ions calculated by NEO for DIII-D shot #160921 for time slot 5100 ms for  $I_{RMP} = 0.001$  kA using equilibrium calculated by linear (in red) and nonlinear M3D-C1 simulations (in blue).

the end of the simulation the fluxes do not change much, which indicates that the MHD calculations have reached a steady-state.

Figure 5 shows the neoclassical particle flux for ions (in blue) and electrons (in red) calculated with NEO for the discharge #160921 after ELM suppression at  $t = 5100$  ms for  $I_{RMP} = 6$  kA using the equilibrium computed by nonlinear M3D-C1 run. It can be seen that the neoclassical particle flux for ions ranges from  $10^{19}$  to  $10^{21}$   $m^{-2} s^{-1}$  and is two orders higher than the electron flux for all  $\psi_{norm}$  values. When the RMP current is reduced to 0 kA (i.e. in the axisymmetric limit), the electron and ion fluxes are equal as expected from intrinsic ambipolarity and indicated with the dashed green curve and triangles magenta markers, respectively in figure 5).

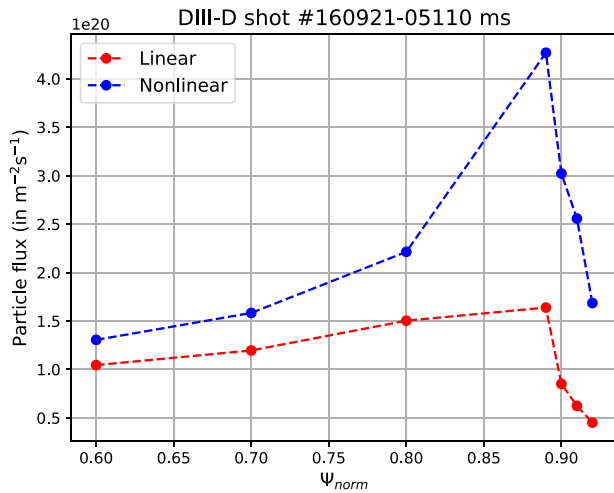


**Figure 8.** Neoclassical particle flux for ions calculated by NEO for DIII-D shot #160921 for time slot 5100 ms for  $I_{RMP} = 6$  kA using equilibrium calculated by linear (in red) and nonlinear M3D-C1 simulations (in blue).

Note that the modest non-axisymmetry introduced by the RMP fields leads to roughly a 100x increase in the calculated ion neoclassical particle flux.

The energy flux for this shot (see figure 6) also follows the same trend as the neoclassical particle flux i.e. on the application of RMPs, the energy flux for both ions (in blue) and electrons (in red) rises significantly from their axisymmetric values. Inferring the particle flux from experiments can be challenging, especially in the edge, due to uncertainties in the particle sources. However, previous estimates of the particle fluxes in comparable RMP DIII-D discharges (see reference [1]) have found total radial ion particle fluxes comparable to the ion neoclassical fluxes that we obtain here. While a quantitative comparison would require detailed particle balance analysis of the shots considered here, comparison with this previous analysis shows that the neoclassical fluxes that we calculate here are on the order of the radial ion fluxes when RMPs are applied and therefore cannot be neglected.

Analysis of the plasma response in the linear calculations shows that the displacement of the magnetic surfaces are sufficiently large that the assumption of linearity is likely breaking down at the edge in these discharges [37]. Therefore, both linear and nonlinear modelling were done for comparison. Nonlinear simulations are computationally more expensive than linear calculations, and therefore understanding when linear results are expected to be accurate will be useful. In both the linear and nonlinear calculations, the initial profiles, equilibrium, and transport parameters were the same.

Figure 7 shows the NEO results for #160921 assuming  $I_{RMP} = 0.001$  kA which is sufficiently small that we would expect linear and nonlinear calculations to yield nearly identical results. As can be seen in the figure, at low  $I_{RMP}$  values, the equilibrium obtained using linear and nonlinear M3D-C1 runs yield similar neoclassical ion particle flux results (<22%) for all radial locations. As the RMP current is increased to the experimental value of 6 kA, the difference in neoclassical particle fluxes obtained becomes more pronounced. For example

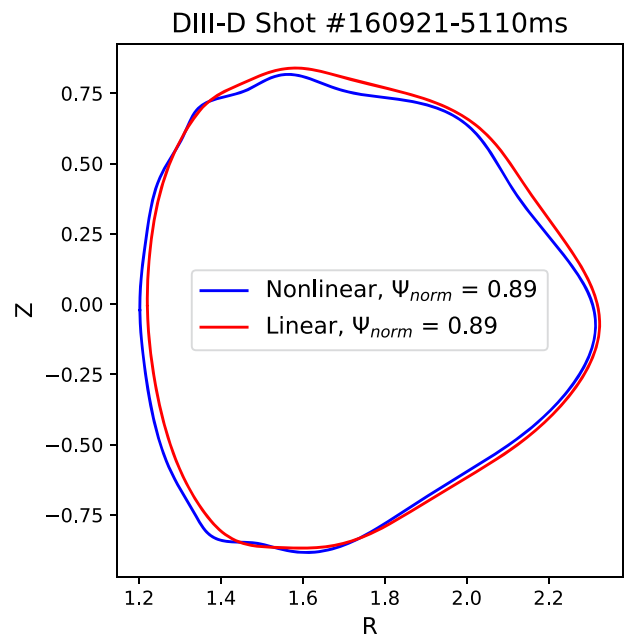
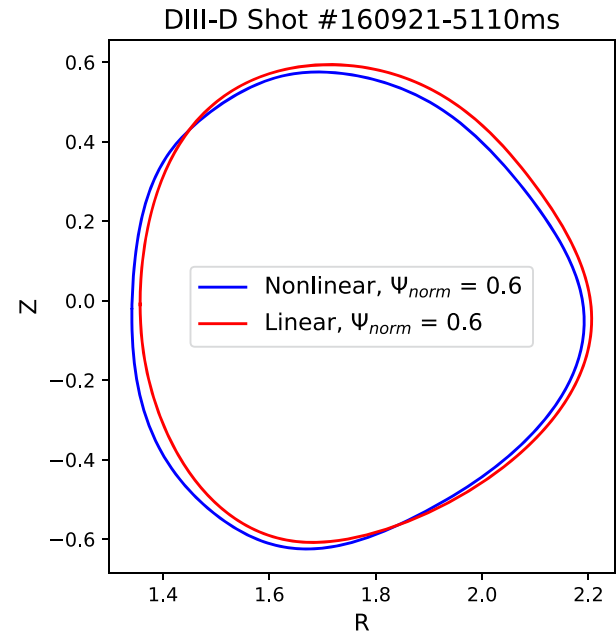


**Figure 9.** Comparison of isotherms for DIII-D shot #160921 at time slot 5100 ms for  $I_{RMP} = 6$  kA (scaled by an additional factor of 10 for better visibility) at  $\psi_{norm} = 0.6$  (top) and  $\psi_{norm} = 0.89$  (bottom) for linear (in red) and nonlinear (in blue) M3D-C1 simulations. Reprinted (figure) with permission from [36], Copyright (2015) by the American Physical Society.

at  $\psi_{norm} = 0.89$ , the difference in the fluxes increases to 160% (see figure 8)

In the 6 kA case, an examination of the transport coefficients calculated by NEO shows that the difference between the fluxes in the linear and nonlinear cases is dominantly due to the differences in the magnetic geometry (explained in the next paragraph). It should be noted that two different nonlinear M3D-C1 calculations were performed one with  $I_{RMP} = 0.001$  kA (figure 7) and  $I_{RMP} = 6$  kA (figure 8) with the same physics model. The above results indicate that

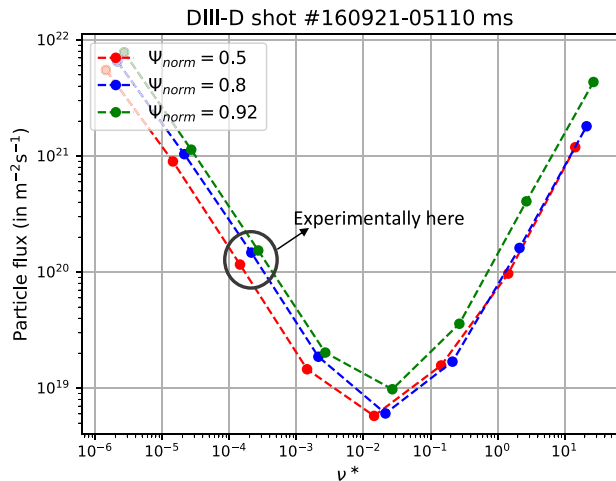


**Figure 10.** Neoclassical particle flux vs collisionality for ions calculated by NEO for DIII-D shot #160921 for time slot 5100 ms for  $I_{RMP} = 6$  kA at using equilibrium calculated by nonlinear M3D-C1 simulations at  $\psi_{norm} = 0.5$  (in red),  $\psi_{norm} = 0.8$  (in blue) and  $\psi_{norm} = 0.92$  (in green).

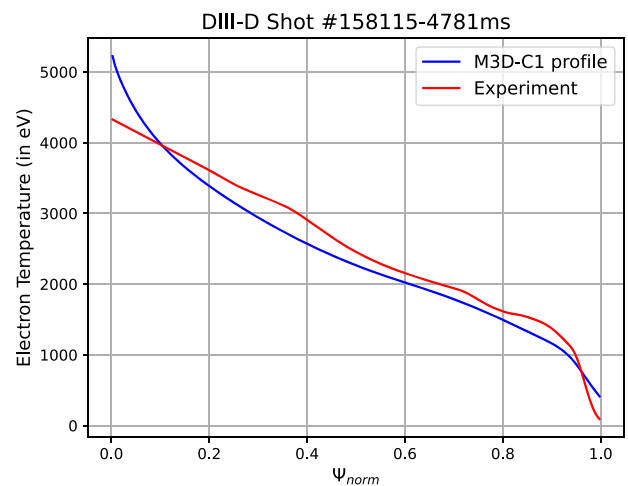
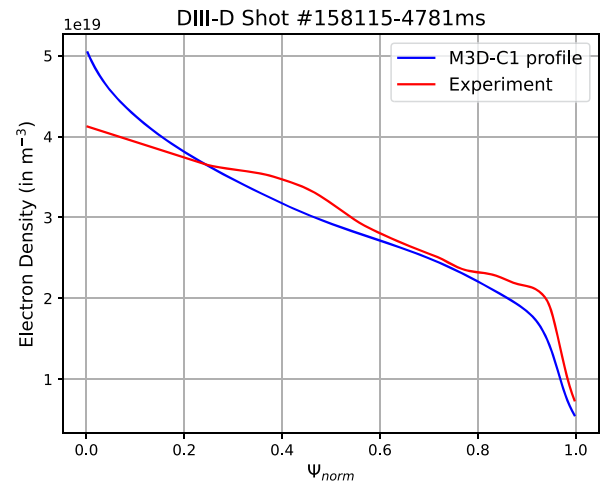
at experimentally relevant RMP current values, perturbation theory is evidently breaking down, and that, it is necessary to do nonlinear MHD simulation to capture this behaviour and get reliable values of neoclassical transport properties.

Figure 9 shows the isotherms for DIII-D shot #160921 at 5110 ms for  $I_{RMP} = 6$  kA at  $\psi_{norm} = 0.6$  and  $\psi_{norm} = 0.89$  for linear and nonlinear M3D-C1 runs. At  $\psi_{norm} = 0.6$ , perturbations in the isotherms for linear and nonlinear M3D-C1 are similar, thus the fluxes obtained are also close to each other (see figure 8). At  $\psi_{norm} = 0.89$ , the perturbation of isotherm for the nonlinear case is larger than linear case, which intuitively would imply higher nonlinear fluxes, this trend is well observed in the neoclassical fluxes calculated at this radial position.

Figure 10 shows the effect of collisionality on 3D neoclassical particle fluxes at different  $\psi_{norm}$  values for DIII-D discharge #160921 at  $I_{RMP} = 6$  kA. The different transport regimes can be well identified from this plot and it can be seen that, in the experiment  $1/\nu$  regime is observed. It can be also inferred from the figure that in  $1/\nu$  regime as the collisionality is increased the particle flux should decrease, which is infact also seen during the experiments in DIII-D [38].

### 3.2. DIII-D discharge #158115

This is an H-mode discharge in which both sets of I-coils were used and operated at  $n = 2$  with  $I_{RMP} = 4$  kA. The relative phase of upper and lower I coil are modulated sinusoidally at a frequency of 1 Hz. Previous work [11, 12, 36, 39] performed on this shot included studies on understanding the dynamics of ELM suppression. It was found that the plasma response and the observation of ELM suppression were strongly correlated with the relative phasing of the coil rows, with the maximum observed magnetic plasma response, maximum particle transport, and observation of ELM suppression all occurring near  $0^\circ$  of relative phase (even parity). For this study, we consider how the neoclassical fluxes are expected to change as a function



**Figure 11.** Comparison of electron density profile (top) and electron temperature profile (bottom) used in linear and nonlinear M3D-C1 runs (in blue) with the experimental profiles (in red) for DIII-D shot #158115 at  $t = 4781$  ms.

of the applied RMP spectrum. To do this, we hold the initial axisymmetric equilibrium fixed (here using the profiles from  $t = 4781$  ms, during an ELM-suppressed period) and calculate the perturbed equilibrium and resulting neoclassical fluxes as the RMP phasing is changed. For time slot  $t = 4781$  ms, the toroidal magnetic field  $B_T = 1.95$  T, line averaged density  $\langle n_e \rangle = 3.3 \times 10^{19} \text{ m}^{-3}$ , plasma current  $I_p = 1.35$  MA,  $q_{95} = 4.2$ , and  $\beta_N = 1.9$ . Model density and temperature profiles consistent with the density and heat sources used for the nonlinear M3D-C1 runs along with the experimental profiles for this discharge are shown in figure 11).

To ensure that the nonlinear MHD calculations for DIII-D shot #158115 at  $I_{RMP} = 4$  kA reached a steady-state, we have repeated the analysis done in figure 4 for this discharge as well.

The focus of the phase study performed here is to analyse the correlation between the RMP phasing and the calculated neoclassical particle flux. The equilibria are calculated with nonlinear MHD using M3D-C1 at different phasings ( $\Delta\phi$ ) for  $I_{RMP} = 4$  kA.  $\Delta\phi$  in our study ranges from  $0^\circ$  to  $120^\circ$ . As the temperature and density profiles were constant for each of the equilibrium, any difference in between them owe to the difference in the amplitude of helical harmonics of RMP field.



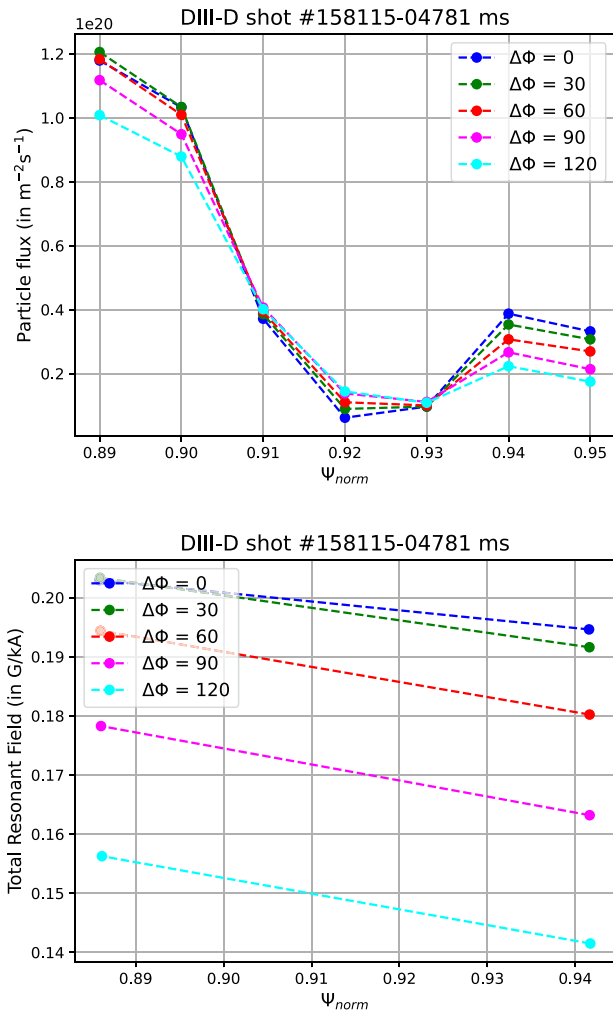


**Figure 12.** Neoclassical particle flux for ions calculated by NEO using equilibrium calculated by nonlinear M3D-C1 (top) and total resonant field (bottom) for DIII-D shot #158115 for time slot 4781 ms at  $I_{\text{RMP}} = 4$  kA for different phasing ( $\Delta\phi$ ).  $\Delta\phi = 0$  (in blue),  $\Delta\phi = 30$  (in green),  $\Delta\phi = 60$  (in red),  $\Delta\phi = 90$  (in magenta), and  $\Delta\phi = 120$  (in cyan).

Figure 12 (top) shows the neoclassical particle flux calculated by NEO for #158115 at different values of  $\Delta\phi$ . It is found that as  $\Delta\phi$  increases, the neoclassical particle flux value decreases in most of the edge region (except  $0.91 \leq \psi_{\text{norm}} \leq 0.93$ ). For example, at  $\psi_{\text{norm}} = 0.94$ , neoclassical particle flux at  $\Delta\phi = 0^\circ$  is  $3.87 \times 10^{20} \text{ m}^{-2} \text{ s}^{-1}$ , which reduces to  $3.07 \times 10^{19} \text{ m}^{-2} \text{ s}^{-1}$  at  $\Delta\phi = 60^\circ$  and further declines to  $2.23 \times 10^{19} \text{ m}^{-2} \text{ s}^{-1}$  at  $\Delta\phi = 120^\circ$ . Figure 12 (bottom) shows the plot for total resonant field and we see a similar trend as neoclassical particle flux i.e. the amplitude of resonant helical harmonics is largest for  $\Delta\phi = 0^\circ$  which reduces as  $\Delta\phi$  increases.

A clear correlation between phasing and particle flux was also experimentally observed (see figure 13) by Nazikan *et al* in reference [36]. As can be seen in figure 13, the pedestal density in the experiment rises and falls significantly as  $\Delta\phi$  is changed in time, with the largest reduction in density occurring near  $\Delta\phi = 0$  (corresponding to  $t_0$  and  $t_3$  in the plot). This is in agreement with the finding that the neoclassical fluxes are

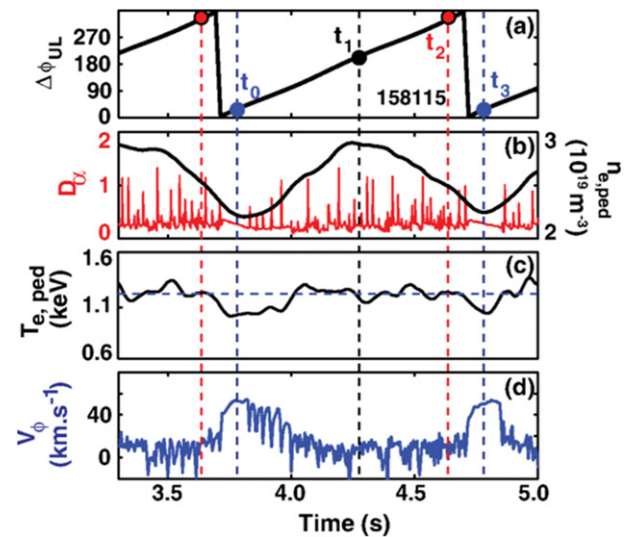


**Figure 13.** Pedestal bifurcations with slowly varying resonant fields. (a) Upper and lower row I-coil relative phase. (b)  $D_\alpha$  light near the outer strike point (red) and pedestal density  $n_{e,\text{ped}}$  (black). (c) Pedestal electron temperature  $T_{e,\text{ped}}$ . (d) Edge impurity velocity in the co-IP direction. (Copyright: Reprinted, with permission, from reference [36]).

maximum at  $\Delta\phi = 0$  in our calculations. We note that there is also a brief window of ELM suppression around  $\Delta\phi = 0$ , as can be seen from the pause in  $D_\alpha$  emission there; however, this brief ELM suppression window does not itself appear to have an appreciable effect on the pedestal density.

#### 4. Conclusions and discussions

An efficient method has been developed in this work for calculating the steady-state neoclassical transport in realistic perturbed tokamak geometry. The analysis of DIII-D discharges #160921 and #158115 shows that modest RMP fields with  $\delta B/B \sim 10^{-3}$  can increase neoclassical fluxes in the edge by more than an order of magnitude, putting these fluxes into the range of the radial fluxes inferred in similar discharges. We find that these neoclassical calculations reproduce the dominant features of the observed particle transport including the dependence on the applied RMP spectrum and the reduction of the fluxes at higher collisionality. This strongly suggests that neoclassical transport is an important transport mechanism in the H-mode edge in the presence of RMPs, which has implications for understanding the evolution of the pedestal structure under these conditions. Our findings do not exclude the possibility of enhanced turbulent transport with RMPs, but rather emphasize that the enhancement of neoclassical transport is important and cannot be neglected.

Flux calculations in DIII-D #160921 showed that nonlinear MHD simulations are essential at high RMPs to satisfactorily model the perturbed magnetic geometry in the pedestal region. The neoclassical fluxes calculated here cannot depend directly on the resonant harmonics of the perturbed field, because the surface geometry provided as input to NEO excludes magnetic islands and stochasticity by construction. However, a clear




correlation between the resonant harmonics of the perturbed field and the calculated neoclassical fluxes is observed in the phase study for the shot #158115. The occurrence of density pump-out which is marked by higher particle flux during RMP ELM-suppressed phase, was also confirmed for shot #158115 using the same temperature and density profile for different phases in the NEO calculations.

As mentioned earlier in the paper, surface-averaged formulation of the DKE employed by NEO and other neoclassical codes cannot treat islands and stochasticity. This limitation requires us to use isotherms of  $T_e$  to give the set of closed surfaces that best approximate the M3D-C1 magnetic field, which may have magnetic islands and stochasticity in some regions. In doing so, we exclude transport effects resulting from nonintegrable magnetic geometry, and capture only the effects due to the ‘kinking’ of surfaces. (The M3D-C1 calculation itself does self-consistently include parallel thermal transport across islands and stochastic regions, but these are not added to the neoclassical fluxes presented here.) In many cases this may be adequate, since strong  $T_e$  gradients observed experimentally suggest that magnetic geometry in the pedestal remains nearly integrable over much of the volume in reality (possibly excluding the outer 2% or so of the magnetic flux, or islands near the top of the pedestal or on interior rational surfaces). However, the extension of drift kinetics to non-integrable field geometries is an area of active research and should be considered in the future.

## Acknowledgments

The work was performed at Princeton Plasma Physics Laboratory, which is managed by Princeton University under Contract No. DE-AC02-09CH11466. This work is supported by the Department of Energy under Award Number DE-FG02-95ER54309 and DOE Early Career Research Grant.

## ORCID iDs

Priyanjana Sinha  <https://orcid.org/0000-0002-0567-0279>  
 Nathaniel M. Ferraro  <https://orcid.org/0000-0002-6348-7827>  
 Emily Belli  <https://orcid.org/0000-0001-7947-2841>

## References

- [1] Stacey W.M., Groebner R.J. and Evans T. 2012 Non-diffusive transport in the tokamak edge pedestal *Nucl. Fusion* **52** 114020
- [2] Groebner R. 1993 An emerging understanding of H-mode discharges in tokamaks\* *Phys. Fluids B* **5** 2343–54
- [3] Itoh S.-I. and Itoh K. 1988 Model of LtoH-mode transition in tokamak *Phys. Rev. Lett.* **60** 2276
- [4] Wade M. *et al* 2015 Advances in the physics understanding of ELM suppression using resonant magnetic perturbations in DIII-D *Nucl. Fusion* **55** 023002
- [5] Fitzpatrick R. 2020 Theory of edge localized mode suppression by static resonant magnetic perturbations in the DIII-D tokamak *Phys. Plasmas* **27** 042506
- [6] Thornton A., Kirk A., Cahyna P., Chapman I., Harrison J., Liu Y., Team M. *et al* 2014 The effect of resonant magnetic perturbations on the divertor heat and particle fluxes in mast *Nucl. Fusion* **54** 064011
- [7] Nardon E. *et al* 2007 Edge localized modes control by resonant magnetic perturbations *J. Nucl. Mater.* **363–365** 1071–5
- [8] Evans T. *et al* 2008 RMP ELM suppression in DIII-D plasmas with ITER similar shapes and collisionalities *Nucl. Fusion* **48** 024002
- [9] Burrell K. *et al* 2005 ELM suppression in low edge collisionality H-mode discharges using  $n = 3$  magnetic perturbations *Plasma Phys. Control. Fusion* **47** B37
- [10] Cui L. *et al* 2017 The energy confinement response of DIII-D plasmas to resonant magnetic perturbations *Nucl. Fusion* **57** 116030
- [11] Paz-Soldan C. *et al* 2015 Observation of a multimode plasma response and its relationship to density pumpout and edge-localized mode suppression *Phys. Rev. Lett.* **114** 105001
- [12] Hu Q., Nazikian R., Grierson B., Logan N., Park J.-K., Paz-Soldan C. and Yu Q. 2019 The density dependence of edge-localized-mode suppression and pump-out by resonant magnetic perturbations in the DIII-D tokamak *Phys. Plasmas* **26** 120702
- [13] Evans T.E. *et al* 2006 Edge stability and transport control with resonant magnetic perturbations in collisionless tokamak plasmas *Nat. Phys.* **2** 419–23
- [14] Callen J., Hegna C. and Cole A. 2013 Magnetic-flutter-induced pedestal plasma transport *Nucl. Fusion* **53** 113015
- [15] Liu Y., Paz-Soldan C., Li L. and Sun Y. 2020 Role of 3D neoclassical particle flux in density pump-out during elm control by RMP in DIII-D *Nucl. Fusion* **60** 036018
- [16] Hager R., Chang C., Ferraro N. and Nazikian R. 2020 Gyrokinetic understanding of the edge pedestal transport driven by resonant magnetic perturbations in a realistic divertor geometry *Phys. Plasmas* **27** 062301
- [17] Wang S. *et al* 2018 Investigation of RMP induced density pump-out on east *Nucl. Fusion* **58** 112013
- [18] Mordijck S. *et al* 2012 Changes in particle transport as a result of resonant magnetic perturbations in DIII-D *Phys. Plasmas* **19** 056503
- [19] Wilcox R. *et al* 2016 Evidence of toroidally localized turbulence with applied 3D fields in the DIII-D tokamak *Phys. Rev. Lett.* **117** 135001
- [20] Holod I., Lin Z., Taimourzadeh S., Nazikian R., Spong D. and Wingen A. 2016 Effect of resonant magnetic perturbations on microturbulence in DIII-D pedestal *Nucl. Fusion* **57** 016005
- [21] Jardin S.C., Breslau J. and Ferraro N. 2007 A high-order implicit finite element method for integrating the two-fluid magnetohydrodynamic equations in two dimensions *J. Comput. Phys.* **226** 2146–74
- [22] Jardin S., Ferraro N., Luo X., Chen J., Breslau J., Jansen K. and Shephard M. 2008 The M3D-C1 approach to simulating 3D 2-fluid magnetohydrodynamics in magnetic fusion experiments *J. Phys.: Conf. Ser.* **125** 012044
- [23] Belli E. and Candy J. 2008 Kinetic calculation of neoclassical transport including self-consistent electron and impurity dynamics *Plasma Phys. Control. Fusion* **50** 095010
- [24] Belli E.A. and Candy J. 2015 Neoclassical transport in toroidal plasmas with nonaxisymmetric flux surfaces *Plasma Phys. Control. Fusion* **57** 054012
- [25] Belli E. and Candy J. 2011 Full linearized Fokker–Planck collisions in neoclassical transport simulations *Plasma Phys. Control. Fusion* **54** 015015
- [26] Candy J. and Belli E.A. 2015 Non-axisymmetric local magnetostatic equilibrium *J. Plasma Phys.* **81** 905810323

- [27] Calvo I., Parra F.I., Velasco J.L. and Alonso J.A. 2013 Stellarators close to quasisymmetry *Plasma Phys. Control. Fusion* **55** 125014
- [28] Parra F.I. and Catto P.J. 2009 Vorticity and intrinsic ambipolarity in turbulent tokamaks *Plasma Phys. Control. Fusion* **51** 095008
- [29] Callen J., Cole A. and Hegna C. 2009 Toroidal flow and radial particle flux in tokamak plasmas *Phys. Plasmas* **16** 082504
- [30] Jardin S.C. 2004 A triangular finite element with first-derivative continuity applied to fusion MHD applications *J. Comput. Phys.* **200** 133–52
- [31] Ferraro N., Lyons B.C., Kim C.C., Liu Y.-Q. and Jardin S.C. 2018 3D two-temperature magnetohydrodynamic modeling of fast thermal quenches due to injected impurities in tokamaks *Nucl. Fusion* **59** 016001
- [32] Ferraro N.M. and Jardin S.C. 2009 Calculations of two-fluid magnetohydrodynamic axisymmetric steady-states *J. Comput. Phys.* **228** 7742–70
- [33] Luxon J.L. 2002 A design retrospective of the DIII-D tokamak *Nucl. Fusion* **42** 614
- [34] Orlov D.M. *et al* 2016 Suppression of type-I ELMs with reduced RMP coil set on DIII-D *Nucl. Fusion* **56** 036020
- [35] Moyer R.A. *et al* 2017 Validation of the model for ELM suppression with 3D magnetic fields using low torque ITER baseline scenario discharges in DIII-D *Phys. Plasmas* **24** 102501
- [36] Nazikian R. *et al* 2015 Pedestal bifurcation and resonant field penetration at the threshold of edge-localized mode suppression in the DIII-D tokamak *Phys. Rev. Lett.* **114** 105002
- [37] Ferraro N. *et al* 2013 Role of plasma response in displacements of the tokamak edge due to applied non-axisymmetric fields *Nucl. Fusion* **53** 073042
- [38] Unterberg E.A. *et al* 2009 Experimental comparison of recycling and pumping changes during resonant magnetic perturbation experiments at low and high collisionality in DIII-D *J. Nucl. Mater.* **390–391** 486–9
- [39] Callen J., Nazikian R., Paz-Soldan C., Ferraro N., Beidler M., Hegna C. and La Haye R. 2016 *Model of  $n = 2$  RMP ELM suppression in DIII-D, UW CPTC Report, 16-4*